Electronic Supplementary Material (ESI) for Physical Chemistry Chemical Physics.

Supporting Information:

Dynamics of a gas phase S_NAr reaction: Non-concerted mechanism despite the Meisenheimer complex being a transition state

Nishant Sharma, Rupayan Biswas, and Upakarasamy Lourderaj*

School of Chemical Sciences, National Institute of Science Education and Research (NISER)

Bhubaneswar, HBNI, P. O. Jatni, Khurda, Odisha, India

E-mail: u.lourderaj@niser.ac.in

1 Computational Details

1.1 Potential Energy Profile

The potential energy profile for the $C_6H_5NO_2 + F^- \longrightarrow C_6H_5F + NO_2^-$ reaction was mapped using different levels of theory. MP2 and DFT methods were employed with 6-31+G*, 6-311++G**,[S1,S2] aug-cc-pVDZ,[S3,S4] and aug-cc-pVTZ[S3,S4] basis sets to compute the energy profile of the reaction. Different DFT functionals such as B3LYP,[S5,S6] M06-2X,[S7] BHandH,[S8] OPBE,[S9–S11] OLYP,[S5,S9,S10] B97-1,[S12] and HCTH407[S13] were used for the study. The nature of the stationary points was established by computing harmonic vibrational frequencies. Intrinsic reaction coordinate (*IRC*) calculations were performed to connect the transition states (TS) to their adjacent minima. All the DFT and MP2 calculations were performed using Gaussian 16 software package.[S14] To validate the energies obtained, single-point energy calculations for the B3LYP/aug-cc-pVDZ equilibrium geometries were performed using DLPNO-CCSD(T) method[S15,S16] with aug-cc-pVDZ, aug-cc-pVTZ, and aug-cc-pVQZ basis sets using ORCA software package.[S17] These energies were then extrapolated to obtain the complete basis set (CBS) limit energies (three-point form)[S18] using the equation,

$$E(X) = E_{\mathrm{CBS}} + Be^{-\alpha X} \tag{1}$$

where X = 2, 3, and 4 and $E(X)$ representing DLPNO-CCSD(T) energies obtained using aug-cc-pVDZ, aug-cc-pVTZ, and aug-cc-pVQZ basis sets respectively. The energies relative to the reactants obtained at the various levels of theory for the different stationary points are given in Table S1. The electronic energies obtained from all the methods were compared to that of the DLPNO-CCSD(T)/CBS level. It can be seen that the B3LYP with 6-31+G*, aug-cc-pVDZ, and aug-cc-pVTZ basis sets have the mean absoluted deviations of less than 1.5 kcal/mol from the DLPNO-CCSD(T)/CBS level. While nearly all the levels of the theory identified all complexes and transition states except the B3LYP/6-311++G** and M06-2X/6-31+G* levels of the theory. At the B3LYP/6-311++G** and M06-2X/6-31+G* levels, **ts2** could not be located and the **idm** was found to have a linear C(sp^2)-H$\cdots$F geometry. It should be pointed that **ts2** and **ido** were

found to be close in energies in all the other methods. However, the *IRC* connected **ts2** with **idm** and **ido** thus enabling a complete round about motion of the F atom from the **idp** to the **mts** along the minimum energy path. Considering the accuracy of the method compared to that of the DLPNO-CCSD(T)/CBS level and computational cost, the B3LYP/6-31+G* level of theory was chosen for *ab initio* classical trajectory simulations.

1.2 Ab initio Classical Trajectory Simulations

Ab initio classical trajectory simulations[S19] at the B3LYP/6-31+G*[S1,S2,S5,S6] level of theory were performed to understand the atomic-level mechanisms and dynamics of the S_NAr reaction. These calculations are computationally very expensive and it is important that optimum level of theory is used in the simulations. The B3LYP/6-31+G* level was found to represent the energetics in close agreement with that of the DLPNO-CCSD(T)/CBS level. Hence, B3LYP/6-31+G* level of theory was used in the ab initio trajectory simulations. The ab initio trajectories were calculated using the VENUS/NWChem software.[S20,S21] A typical trajectory integrated for 4 ps takes a wall time of about 4 days using 32 cores on a 2.60 GHz Intel Xeon processor.

1.2.1 Bimolecular Trajectory Simulations

To understand the atomic-level mechanism of the $C_6H_5NO_2 + F^- \longrightarrow C_6H_5F + NO_2^-$ reaction bimolecular collision trajectories were computed. A complete description of the bimolecular collision dynamics would involve computing numerous trajectories for a range of impact parameters ($b = 0$ to $b = b_{max}$) with random orientations of the reactants. However, this is computationally very expensive. Thus, with the objective to understand the different mechanisms possible and to obtain a qualitative description of the dynamics of the reaction, the trajectories were calculated as described below.

The initial coordinates and momenta for the trajectories were selected using quasi-classical thermal sampling of vibrational and rotational energies at 335 K which is the temperature used in gas phase experiments by Riveros and coworkers.[S22] The trajectories were integrated numerically

for 4 ps using velocity-Verlet algorithm with a timestep of 0.4 fs. The initial separation between $C_6H_5NO_2$ and F^- was set to 10 Å . While a larger initial separation is preferred, a value of 10 Å was chosen to cut down the computational cost. At this separation, the interaction energy for the most attractive, para hydrogen side approach was -2.8 kcal/mol. The impact parameter b was chosen to be zero for effective collisions. A relative translational energy E_{rel} of 0.99 kcal/mol corresponding to the average translational energy at the experimental temperature of 335 K was provided to the reactants. The trajectories were terminated when the separation between the products was greater than 10 Å or after 4 ps of integration time. A total of 395 trajectories were initiated with randomly chosen orientations of F^- about $C_6H_5NO_2$. Out of 395 trajectories, 3 were found to be reactive and gave fluorobenzene and nitrite anion (NO_2^-) as products, 189 trajectories were non-reactive, and the remaining 203 trajectories were trapped till 4 ps of integration time. Although the reaction probability was low, the simulations revealed interesting dynamical pathways followed in the reaction.

1.2.2 Trajectories Initiated at the mts transition state

To understand the post-transition state dynamics and to improve the statistics of reactive trajectories, we have performed classical trajectory simulations initiated at the **mts** transition state. The total energy $E_{\textbf{mts}}$ available at **mts** was calculated by considering average thermal energies available to the reactants $E_{\text{reactants}}$ at 335 K and the potential energy difference between the reactants and **mts** ($\Delta E, 9.1$ kcal/mol) given by

$$E_{\textbf{mts}} = \Delta E + E_{\text{reactants}} = 79.1 \text{ kcal/mol} \tag{2}$$

where, $E_{\text{reactants}}$ is the sum of the average vibrational (including zero-point-energy, 68.04 kcal/mol) and rotational (0.99 kcal/mol) energies for $C_6H_5NO_2$ and the relative translational energies (0.99 kcal/mol) for the reactants at 335 K. The energy at the **mts** was partitioned into

$$E_{\textbf{mts}} = E_{\text{vib}} + E_{\text{rot}} + E_{\text{RC}} \tag{3}$$

where, E_{vib}, E_{rot}, and $E_{\text{RC}} = RT$ are the vibrational, rotational, and reaction coordinate energies at the **mts**. The vibrational energy can then be defined as $E_{\text{vib}} = E_{\textbf{mts}} - E_{\text{rot}} - RT$.

414 trajectories were initiated using microcanonical normal mode sampling algorithm with a vibrational energy of 77.47 kcal/mol. A rotational energy of 0.99 kcal/mol was given to **mts** and an energy of 0.66 kcal/mol was made available to the reaction coordinate. The trajectories were integrated for 1 ps in the forward and 1 ps in the reverse directions for a given set of initial conditions. The direction was defined with respect to sign of momenta. If q_i^f and p_i^f are the coordinate and momentum for the i^{th} component for a trajectory that was integrated in the forward direction, then, $q_i^r = q_i^f$ and $p_i^r = -p_i^f$ are initial coordinate and momentum for the i^{th} component in the reverse direction.

2 Trajectory analysis

2.1 Coordinate system

To understand the mechanism followed by the reaction in different trajectories, the analysis was done using a rotated coordinate system. In this coordinate system, the para-carbon (C1) is set as the origin, the vector connecting C2 and C1 is aligned along the *y*-axis, and the atoms C1, C2, and C3 lie on the *xy*-plane. The new rotated coordinate system is depicted in Figure S8. In the new coordinate system, the atomic-level mechanisms can be easily described by following the positions of only the F atom during the trajectory. The figures that depict the mechanisms of the reaction (F atom Cartesian coordinates) in the manuscript use the rotated coordinate system.

2.2 Dynamical Reaction Pathways

The pathway along intrinsic reaction coordinate (*IRC*) gives the steepest descent path followed in the reaction. However, during the reaction the availability of kinetic energy can open up multitude of dynamical reaction pathways that deviate from the *IRC* path. Therefore, to investigate the

dynamical reaction paths followed in the trajectories, we used the reduced dimensional representation of reaction pathways proposed by Carpenter and coworkers.[S23,S24] The principal component analysis (PCA) was performed on the Cartesian *IRC* to obtain a reduced three dimensional (R3D) representation of the *IRC*. The three largest contributing components (PC1, PC2, and PC3) that represent the *IRC* are given in Figures S3a and S3b. Interestingly, we found that until the **mts**, the *IRC* in the reduced dimensional principle components (PC1, PC2,and PC3) is well represented by the three Cartesian coordinates (x,y,z) of the F atom in the *IRC* (Figure S3c). Thus, since the F atom coordinates represent its realistic positions in the Cartesian space and are easy to comprehend, they are used to describe the *IRC* and trajectories wherever necessary for clarity.

To analyze if an ab initio trajectory follows the *IRC* or deviates from it, the Cartesian coordinates of the trajectory were first projected on to the R3D space defined above by PC1, PC2 and PC3. A representative trajectory and *IRC* in the R3D space are plotted together in Figure S3d for illustration. Then, for each point ($\boldsymbol{q}^i$) in the trajectory the minimum distance (d^i_{min}) of the trajectory point from all the *IRC* points ($\boldsymbol{q}^j$) given by

$$d^i_{\text{min}} = \min(\boldsymbol{q}^i - \boldsymbol{q}^j) \tag{4}$$

in the R3D space was calculated.[S24] This gives the overall deviation of a trajectory from the *IRC* during the course of the reaction. From the geometries of stationary points on the PES, we observed that the typical H$\cdots$F distance in the ion-dipole complexes was 1.5 Å and the sum of van der Waal radii of H and F atoms was 2.5 Å. Thus, a distance of 1.0 Å (2.5 minus 1.5) was used as a cut-off to define qualitatively the *IRC* path region on the PES. A trajectory that deviates (d_{min}) from the *IRC* by more than about 1.0 Å (after the initial approach of the F^- to the nitrobenzene) was categorized as a non-*IRC* trajectory. In roaming trajectories, a d_{min} cut-off of $\sim$ 2.0 Å which is twice the *IRC* cut-off was used. This larger cut-off translates to the system showing large deviation from the *IRC* and skipping the formation of neighboring **id** complexes after the initial formation of an **id** complex. A d_{min} of about 2 Å or more also means that the system accesses the weak

interaction region of the PES with the F atom hovering about the phenyl ring. It should be pointed that the roaming trajectories are a subset of non-*IRC* trajectories. In addition, the closest complex structure (sigma or ion-dipole) to a point on the trajectory was also calculated to identify the regions accessed by the trajectory during the reaction.

The dynamical pathways followed past the **mts** region was also investigated using the PCA analysis. The minimum deviation of the trajectory from the *IRC* reveal that all the trajectories closely followed the MEP with $d_{\min}$ values less than 1 Å.

2.3 Lifetime calculations

The lifetimes of various complexes formed during the reaction were calculated by calculating the time for which the system stayed in a particular complex region of the PES. The criteria used to define the various complex regions are given in Table S2. The criteria were defined by using the geometrical parameters of the complexes and the respective TSs they connect. For example, **idp** complex is connected to the neighboring complexes **idm**, **idm**$'$, and **psc** by the transition states **ts1**, **ts1**$'$, and **ts0** respectively. The geometrical parameters of these two transition states (**ts0**, **ts1**, and **ts1**$'$) define the **idp** intermediate region. In a given trajectory, the system may enter and leave a complex region several times. For every such event, the lifetime of the complex is computed as the difference between the time when system enters and leaves the complex region. The total lifetime of the system in all the complex regions of the PES for a trajectory was calculated by taking the sum of all the lifetimes of the individual complexes during the course of a trajectory. The total lifetime distribution thus obtained is given in Figure S6. In addition, the lifetimes distributions of the complexes formed during the course of the reaction are shown in Figure S7. The lifetimes exhibit non-exponential behavior. The lifetimes of the **ipc** formed just before the dissociation of the NO_2 group via the **mts** was also plotted separately. This distribution was also found to be non-exponential. It can be considered that the unimolecular dissociation from the **ipc** is non-statistical in nature with a fast initial decay followed by a slower decay at longer times.

Table S1: Electronic energies (kcal/mol) of stationary points relative to the reactants obtained at different levels of theory[a]

Method	**idp**	**ts0**	**psc**	**ts1**	**idm**	**ts2**	**ido**	**ts3**	**osc**	**ts4**	**ipc**	**mts**	**P**	**MUD**[b]
B3LYP/6-31+G*	-26.10	-19.70	-23.54	-23.29	-24.54	-20.49	-20.51	-16.24	-20.58	-12.87	-14.34	-9.11	-25.87	1.4
B3LYP/6-311++G**	-27.10	-20.78	-23.62	-24.48	-25.64	–[c]	19.93[d]	-17.52	-20.80	-14.44	-15.82	-10.68	-26.21	
B3LYP/aug-cc-pVDZ	-25.92	-19.59	-23.02	-22.81	-24.43	-20.12	-20.42	-16.08	-20.21	-12.76	-14.11	-9.34	-23.92	1.3
B3LYP/aug-cc-pVTZ	-25.10	-19.04	-22.38	-22.30	-23.65	-19.61	-19.69	-15.65	-19.54	-12.65	-13.97	-9.25	-25.98	1.2
M06-2X/6-31+G*	-26.46	-18.55	-29.80	-25.18	-25.30	–[c]	19.96[d]	-16.33	-27.53	-15.52	-16.86	-15.96	-29.18	
M06-2X/6-311++G**	-27.78	-19.90	-30.09	-26.42	-26.65	-23.62	-23.64	-17.82	-27.92	-17.18	-18.39	-17.65	-29.80	5.0
MP2/aug-cc-pVDZ	-23.22	-10.28	-16.09	-21.72	-21.23	-18.60	-17.09	-8.45	-12.99	-9.92	-5.90	-1.56	-32.51	4.4
BHandH/aug-cc-pVDZ	-31.73	-22.85	-35.81	-29.32	-30.24	-26.70	-26.95	-20.17	-33.32	-18.65	-20.80	-19.20	-23.40	7.7
BHandH/aug-cc-pVTZ	-30.96	-22.42	-36.15	-28.68	-29.51	-26.11	-26.29	-19.89	-33.60	-18.57	-20.78	-20.55	-26.06	7.5
OPBE/aug-cc-pVDZ	-24.41	-18.76	-24.15	-19.82	-22.79	-17.23	-19.08	-14.60	-21.45	-9.63	-12.00	-10.99	-21.51	2.4
HCTH407/aug-cc-pVDZ	-25.34	-20.52	-21.82	-22.04	-23.58	-19.43	-19.78	-16.68	-18.93	-12.59	-13.76	-8.99	-21.20	1.6
OLYP/aug-cc-pVDZ	-23.85	-18.81	-20.65	-20.25	-22.07	-17.54	-18.03	-14.79	-17.65	-10.12	-11.39	-7.77	-22.98	2.0
B97-1/aug-cc-pVDZ	-27.20	-20.62	-25.91	-23.97	-25.72	-21.34	-21.85	-17.18	-23.26	-13.84	-15.37	-12.45	-23.87	2.5
DLPNO-CCSD(T)/CBS	-24.27	-15.80	-19.88	-22.80	-23.76	-20.67	-20.49	-13.80	-18.00	-13.54	-14.17	-10.10	-24.84	
Experiment[e]													-28.7	

[a]Energies do not include zero-point energy.
[b]Mean unsigned deviation(MUD) with respect to the DLPNO-CCSD(T)/CBS level of theory.
[c]Optimized geometry is a minimum where C(sp^2)–H–F is linear.
[d]Geometry optimization results in **idm** stationary point.
[e]Enthalpy of the reaction at 298 K.[S22]

Table S2: Criteria used to define the different complexes regions for the lifetime calculation of the complexes. The criteria were assigned based on the geometrical parameters of the different stationary point structures.

Intermediate	Criteria[a]
idp	d(H9-F) $<$ 2.53 Å and $\angle$C1-H9-F $<$ 62.5° and d(H9-F)*sin($\angle$F-H9-C1) $<$ 1.97Å
psc	d(C1-F) $<$ 2.34 Å and $\angle$H9-C1-F $>$ 60.0°
idm	d(F-H8) $<$ 2.53 Å and d(F-H8)*sin($\angle$F-H8-C5) $<$ 2.19 Å for 0° $<$ $\lvert\angle$F-H8-C5-C4$\rvert$ $<$ 90° (or) d(F-H8) $<$ 2.53 Å and d(F-H8)*sin($\angle$F-H8-C5) $<$ 1.56 Å for 90° $\leq$ $\lvert\angle$F-H8-C5-C4$\rvert$ $\leq$ 180°
idm′	d(F-H10) $<$ 2.53 Å and d(F-H10)*sin($\angle$F-H10-C3) $<$ 1.56 Å for 0° $<$ $\lvert\angle$F-H10-C3-C6$\rvert$ $<$ 90° (or) d(F-H10) $<$ 2.53 Å and d(F-H10)*sin($\angle$F-H10-C3) $<$ 2.19 Å for 90° $\leq$ $\lvert\angle$F-H10-C3-C6$\rvert$ $\leq$ 180°
ido	d(F-H11) $<$ 1.83 for 0° $<$ $\lvert\angle$C3-C6-H11-F$\rvert$ $<$ 35° (or) d(F-H11) $<$ 2.18 for 35° $<$ $\lvert\angle$C3-C6-H11-F$\rvert$ $<$ 73.2°
ido′	d(F-H7) $<$ 1.83 for 0° $<$ $\lvert\angle$C5-C4-H7-F$\rvert$ $<$ 35° (or) d(F-H7) $<$ 2.18 for 35° $<$ $\lvert\angle$C5-C4-H7-F$\rvert$ $<$ 73.2°
osc	d(C4-F) $<$ 2.4 Å and 76.62° $<$ $\angle$F-C4-C2 $<$ 119.47°
osc′	d(C6-F) $<$ 2.4 Å and 76.62° $<$ $\angle$F-C6-C2 $<$ 119.47°
ipc	d(C2-F) $<$ 2.5 Å, d(C2-N) $<$ 1.69 Å, $\angle$C6-C2-F $>$ 71.4 °

[a] d represents bond distances

.

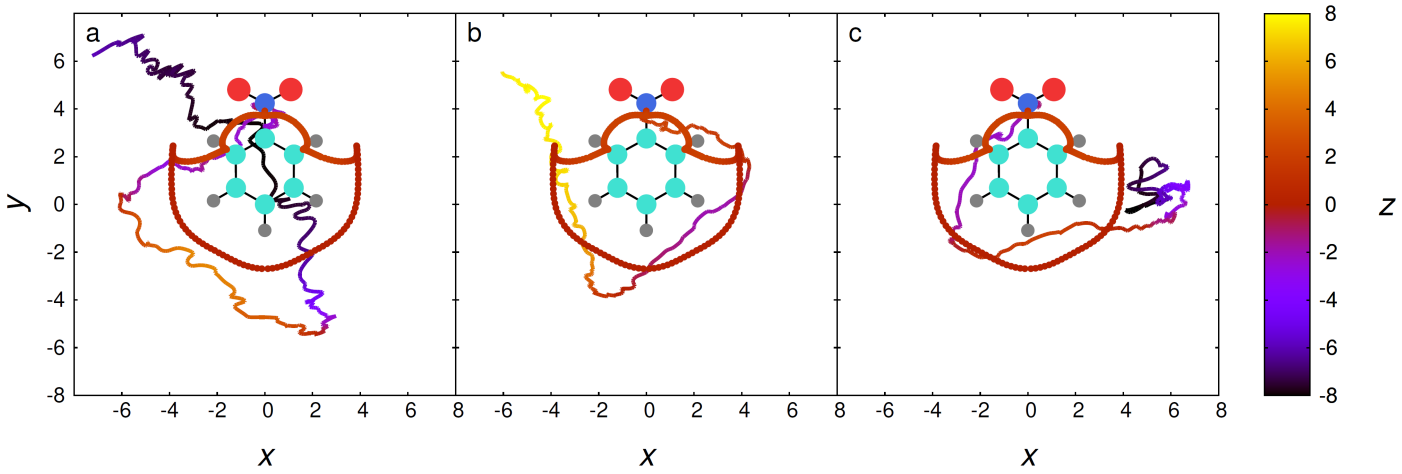

Figure S1: Bimolecular reactive trajectories that show the coordinates (Å) of F atom during the reaction in the rotated coordinate system. The *IRC* path is also shown for clarity.

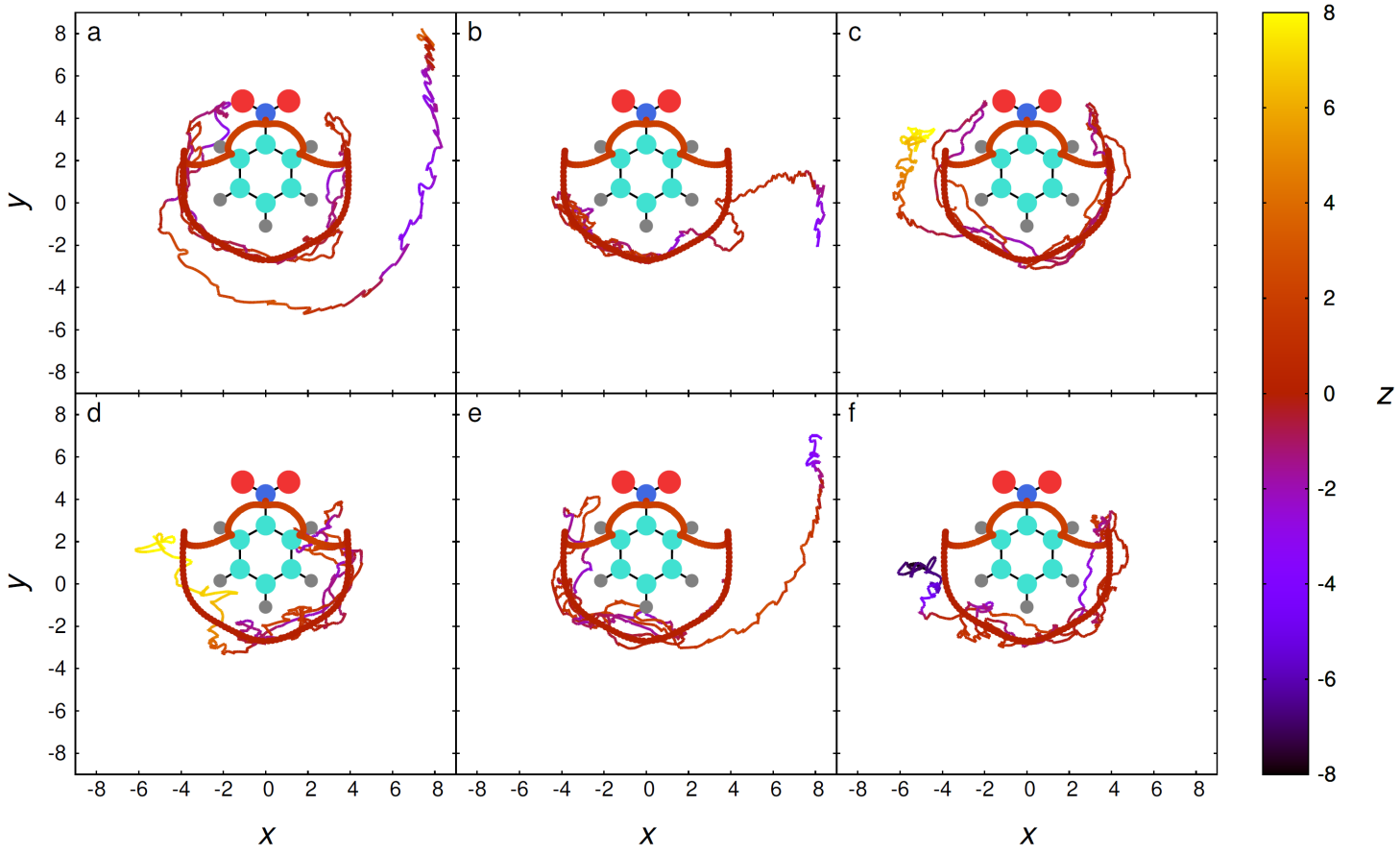

Figure S2: Bimolecular trapped trajectories that show the coordinates (Å) of the F atom during the reaction in the rotated coordinate system. The *IRC* path is also shown for clarity.

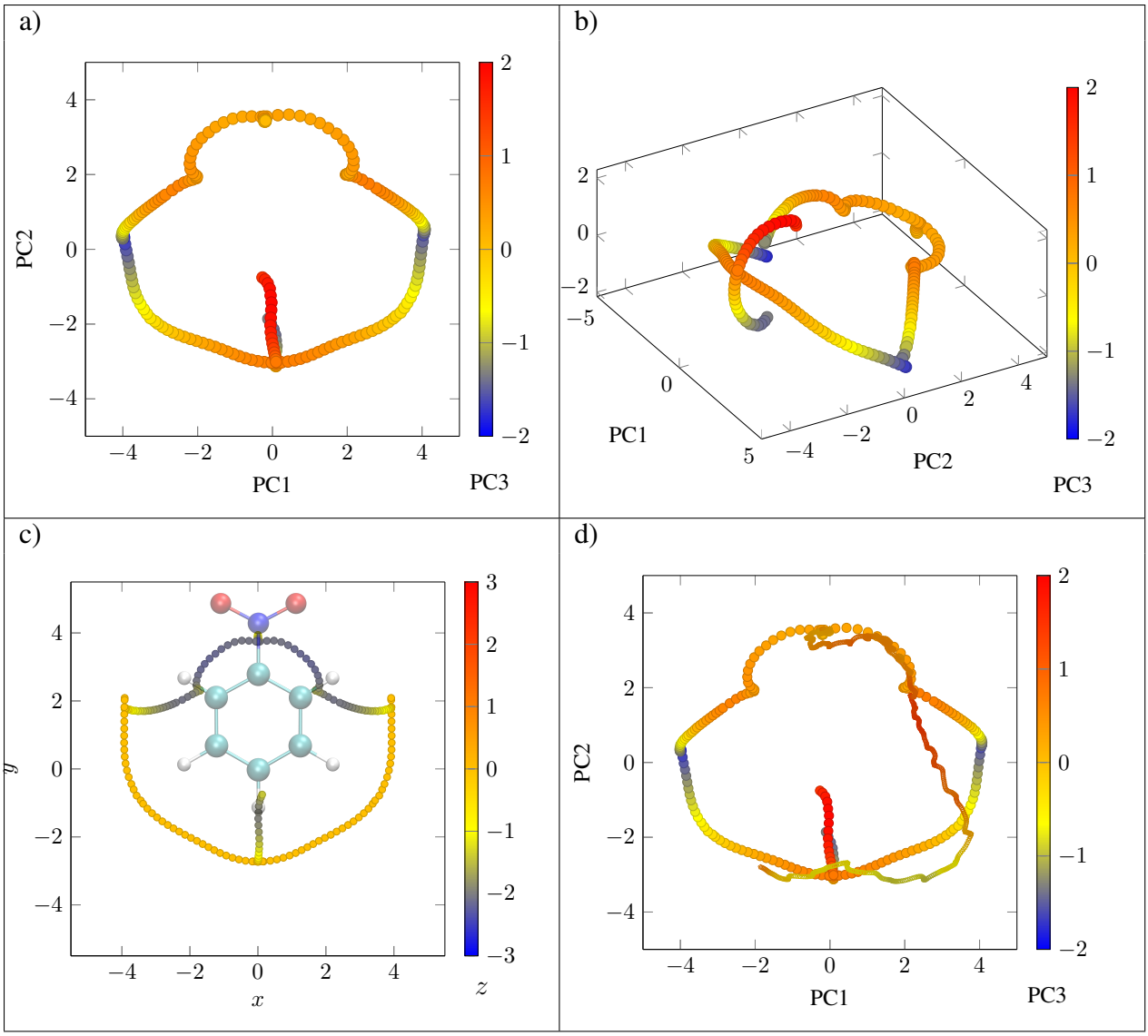

Figure S3: Plot of *IRC* using the three largest principle components (PC1, PC2, and PC3) that represent the *IRC*. (a) Top view and (b) Side view. (c) Cartesian coordinates (Å) of the F atom in the MEP. (d) A representative trajectory and *IRC* in the R3D space.

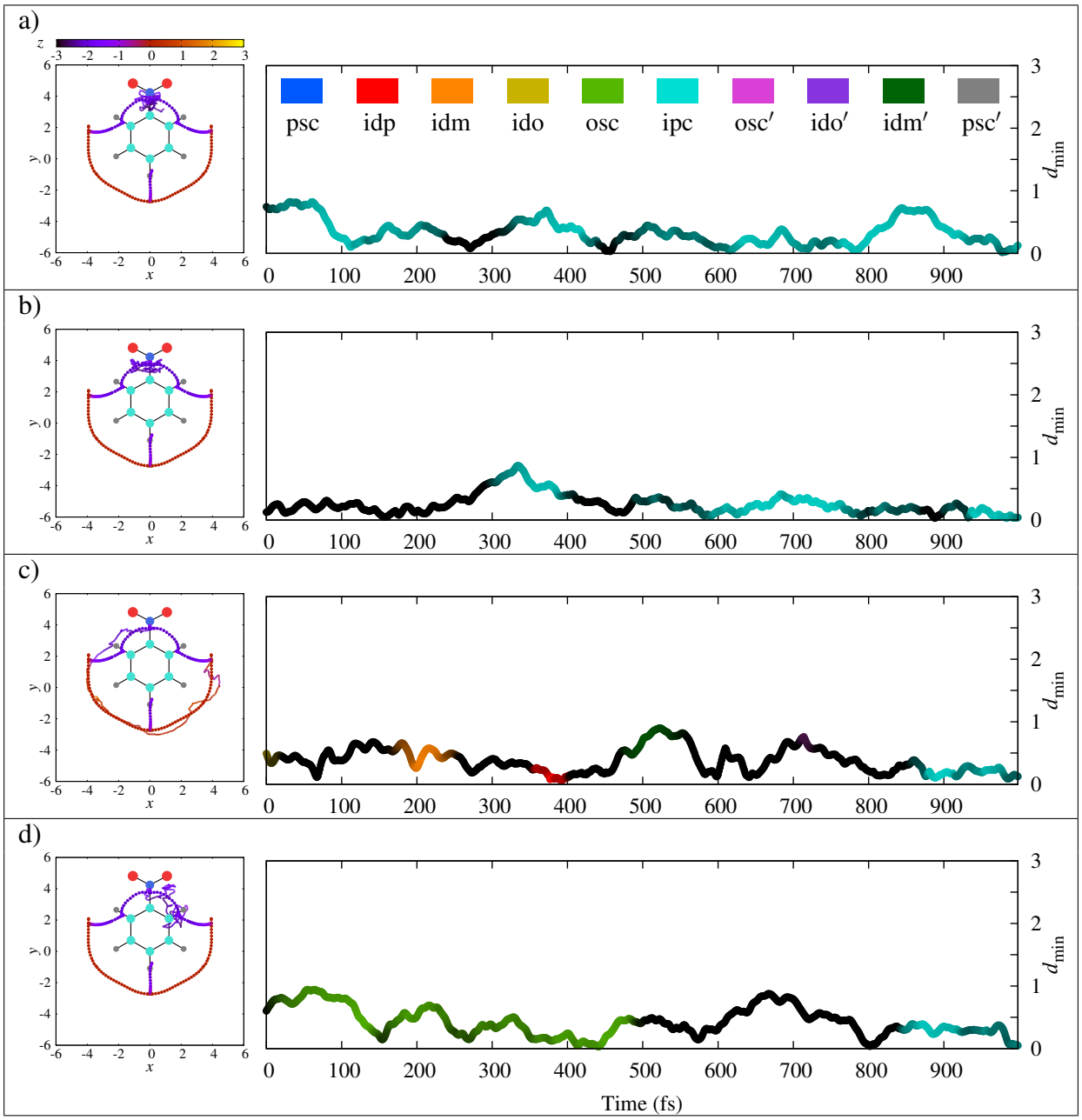

Figure S4: Representative trajectories initiated at **mts** following (a)-(b) *direct-IRC* and (c)-(d) *IRC* pathways. Left: Cartesian coordinates (Å) of the F atom in the trajectory and the *IRC*. Right: Minimum deviation of the trajectory from *IRC* in R3D space. The deviations are less than 1 Å. The color codes indicate that the nearest *IRC* point from the trajectory is a stationary point defined by its color.

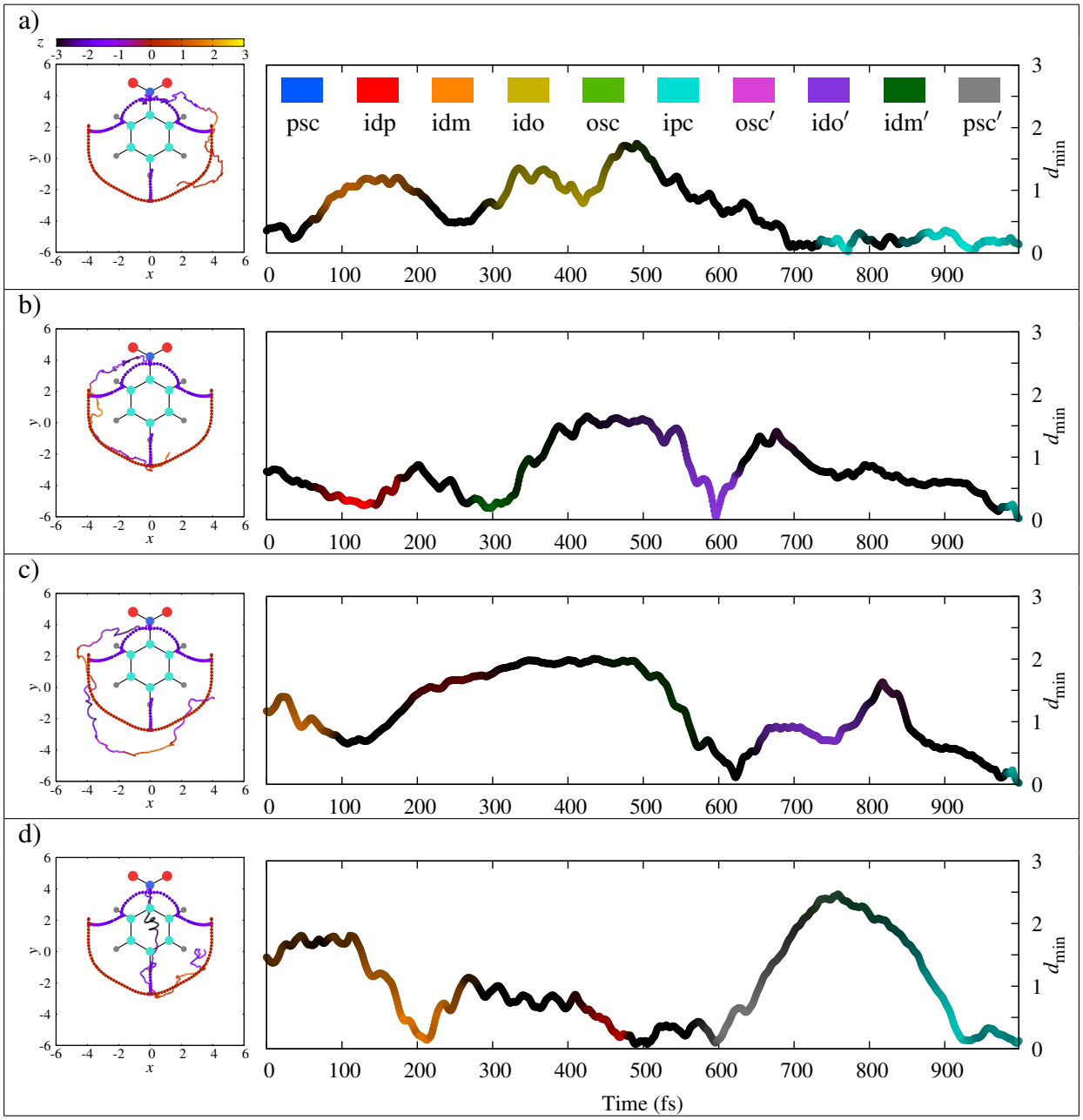

Figure S5: Representative trajectories initiated at **mts** following (a)-(b) *non-IRC* and (c)-(d) *roaming atom* pathways. Left: Cartesian coordinates (Å) of the F atom in the trajectory and the *IRC*. Right: Minimum deviation of the trajectory from *IRC* in R3D space. The color codes indicate that the nearest *IRC* point from the trajectory is a stationary point defined by its color.

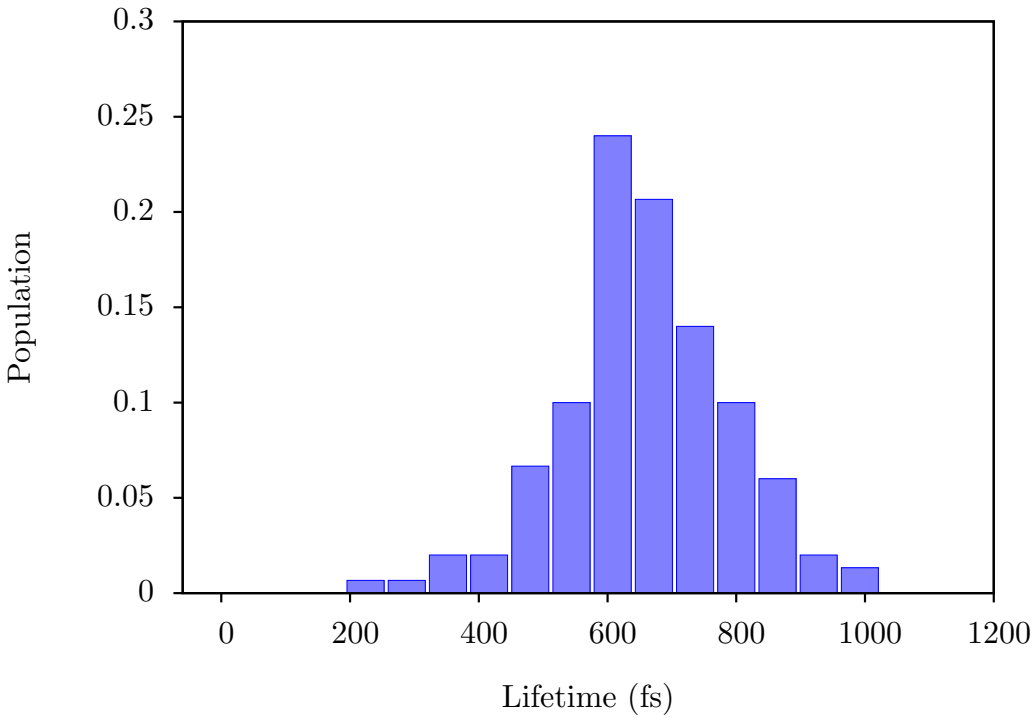

Figure S6: Distribution of the total lifetime of system in the complex region for the 150 reactive trajectories.

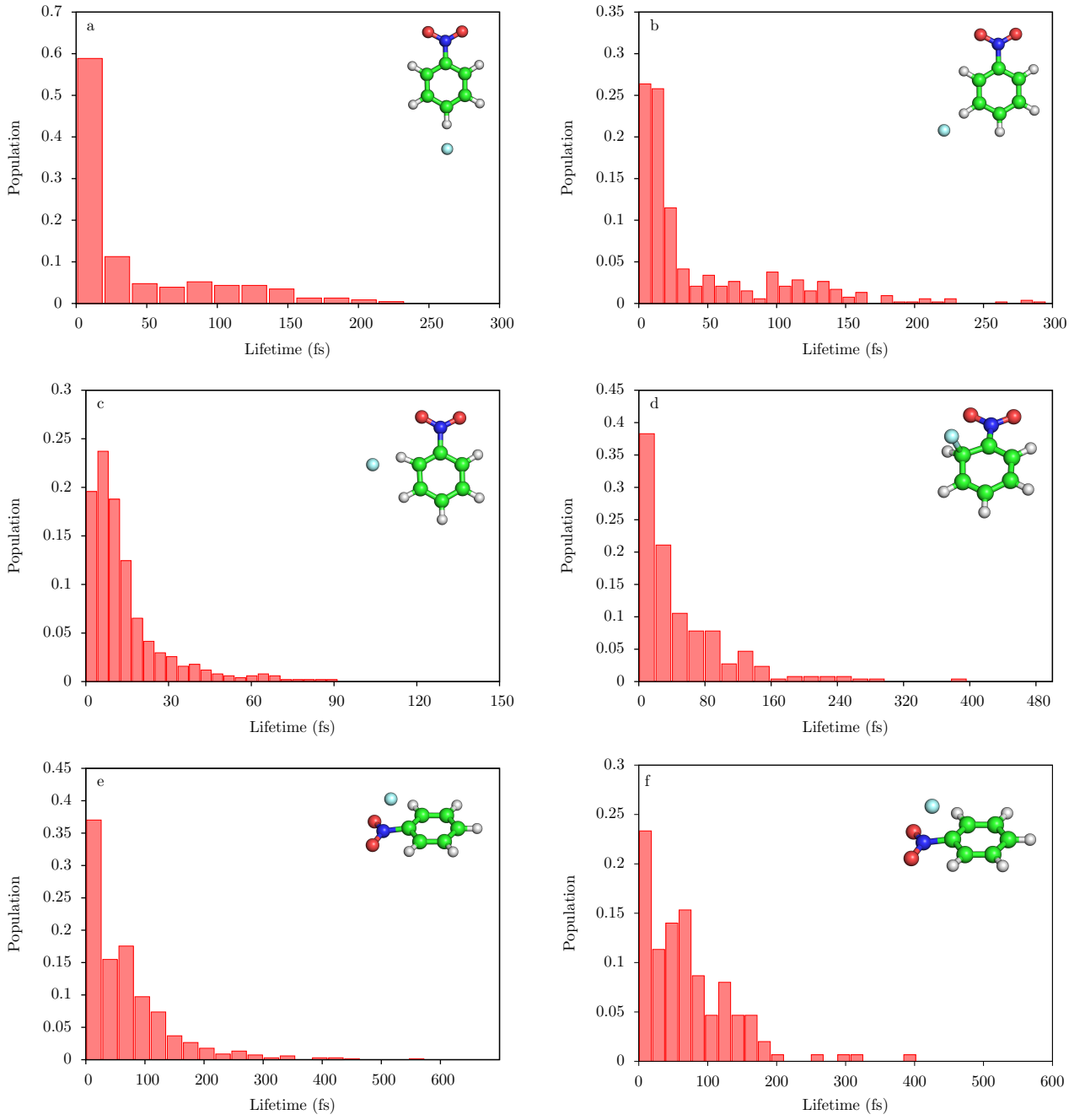

Figure S7: Distribution of lifetime for (a) **idp**, (b) **idm**, (c) **ido**, (d) **osc**, and (e) **ipc** for the 150 reactive trajectories initiated at **mts**. (f) Lifetime distribution for **ipc** formed just before the dissociation of the NO_2 group.

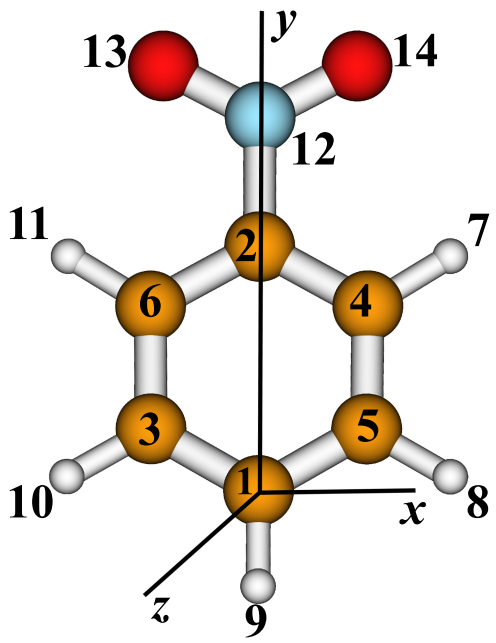

Figure S8: Rotated coordinate system with C1 as the origin.

2.4 Optimized coordinates of stationary points at the B3LYP/6-31+G* level of theory

Nitrobenzene

-436.7699523, No. of imaginary frequencies = 0

C	-0.001358	0.000000	0.052022
C	-0.000530	0.000000	1.447314
C	1.225996	0.000000	2.111904
C	2.421121	0.000000	1.384564
C	2.395547	0.000000	-0.014253
C	1.177539	0.000000	-0.694333
H	-0.940504	0.000000	1.986181
H	1.247213	0.000000	3.197907
H	3.373252	0.000000	1.908312
H	3.324134	0.000000	-0.577793
H	1.129382	0.000000	-1.776742
N	-1.293785	0.000000	-0.658904
O	-2.322354	0.000000	0.019437
O	-1.271596	0.000000	-1.890814

F^-

-99.8596977

idp

-536.6712445, No. of imaginary frequencies = 0

C	1.169454	0.000000	-0.695259
C	-0.023190	0.000000	0.041044
C	-0.014901	0.000000	1.442641
C	1.212158	0.000000	2.102520
C	2.430688	0.000000	1.400447
C	2.379651	0.000000	-0.004942
N	-1.296430	0.000000	-0.664309
O	-1.288403	0.000000	-1.904516
O	-2.343603	0.000000	0.000227

H	−0.955734	0.000000	1.981866
H	1.233089	0.000000	3.190196
H	3.424551	0.000000	1.951014
H	3.312865	0.000000	−0.564037
H	1.127632	0.000000	−1.778856
F	4.815207	0.000000	2.721267

idm

−536.6687649, No. of imaginary frequencies = 0

C	−0.061233	−0.788750	0.000000
C	−1.461437	−0.772700	0.000000
C	−2.101148	0.465240	0.000000
C	−1.347966	1.648145	0.000000
C	0.054805	1.632539	0.000000
C	0.697237	0.388541	0.000000
H	−2.013953	−1.704691	0.000000
H	−3.189081	0.503650	0.000000
H	−1.853169	2.612063	0.000000
H	0.626354	2.613825	0.000000
H	1.780210	0.328872	0.000000
N	0.618255	−2.087335	0.000000
F	1.266790	4.078024	0.000000
O	1.853829	−2.108714	0.000000
O	−0.074320	−3.116515	0.000000

ido

−536.662339, No. of imaginary frequencies = 0

C	−0.856965	0.001070	0.000000
C	0.538079	−0.041033	0.000000
C	1.266555	−1.242059	0.000000
C	0.570594	−2.445970	0.000000
C	−0.834897	−2.440371	0.000000
C	−1.529491	−1.232031	0.000000
N	1.309412	1.214937	0.000000

O	0.701844	2.282282	0.000000
O	2.551471	1.135522	0.000000
H	2.349908	-1.213934	0.000000
H	1.118997	-3.385728	0.000000
H	-1.377202	-3.384769	0.000000
H	-2.614722	-1.178897	0.000000
H	-1.539791	0.887627	0.000000
F	-3.178329	1.349736	0.000000

osc

-536.6624451, No. of imaginary frequencies = 0

C	-0.149975	-0.144782	-0.303602
C	-0.078644	0.142299	1.134037
C	1.233699	-0.207225	1.714904
C	2.341129	-0.371178	0.930187
C	2.258331	-0.356358	-0.498373
C	1.014481	-0.274472	-1.091400
H	-0.940614	-0.223916	1.689201
H	1.309495	-0.250393	2.799629
H	3.308390	-0.552031	1.401152
H	3.155367	-0.466898	-1.102993
H	0.897659	-0.344198	-2.167752
N	-1.411905	-0.259195	-0.907617
O	-1.491360	-0.471918	-2.149362
O	-2.448070	-0.166885	-0.199608
F	-0.264972	1.658639	1.370963

ipc

-536.6524977, No. of imaginary frequencies = 0

C	1.217376	-0.057988	-0.713936
C	0.013758	-0.124423	-0.007980
C	-0.008114	-0.053486	1.387005
C	1.198771	0.015832	2.081733
C	2.418402	0.047412	1.394298

C	2.416339	0.011354	−0.005608
N	−1.256588	0.013164	−0.749290
O	−1.199879	0.148338	−1.975792
O	−2.295993	0.152688	−0.096638
H	−0.961200	−0.094306	1.899102
H	1.186301	0.043231	3.169941
H	3.357373	0.101420	1.941893
H	3.357476	0.035269	−0.552229
H	1.193893	−0.102196	−1.795499
F	−0.710776	−2.241218	−0.425564

ts0

−536.6610478, No. of imaginary frequencies = 1

C	2.387103	−0.289593	0.072976
C	1.238819	−0.092231	−0.678541
C	−0.001677	0.007705	−0.023647
C	−0.083774	−0.081450	1.377431
C	1.075245	−0.278899	2.112259
C	2.331387	−0.370406	1.479182
N	−1.202357	0.185664	−0.796973
O	−1.114024	0.253091	−2.038196
F	3.623317	1.395821	2.301208
O	−2.294905	0.262754	−0.202516
H	−1.052232	0.001645	1.857296
H	1.024280	−0.329612	3.196005
H	3.221511	−0.574507	2.052868
H	3.351922	−0.348597	−0.422322
H	1.274352	−0.017326	−1.759379

ts1

−536.6667649, No. of imaginary frequencies = 1

C	1.772837	0.821322	0.000000
C	1.401480	−0.524358	0.000000
C	0.038069	−0.840434	0.000000

C	−0.954717	0.152609	0.000000
C	−0.567363	1.490555	0.000000
C	0.795746	1.824176	0.000000
N	−0.354906	−2.246916	0.000000
O	0.534128	−3.112218	0.000000
O	−1.561438	−2.524553	0.000000
F	−0.735122	4.275699	0.000000
H	−1.999110	−0.138549	0.000000
H	−1.237077	2.357453	0.000000
H	1.003525	2.893666	0.000000
H	2.829612	1.080779	0.000000
H	2.136536	−1.320795	0.000000

ts2

−536.6623105, No. of imaginary frequencies = 1

C	0.436561	1.816085	0.000000
C	−0.424814	0.707966	0.000000
C	0.157932	−0.559651	0.000000
C	1.549297	−0.754762	0.000000
C	2.379339	0.360825	0.000000
C	1.820459	1.651102	0.000000
N	−0.695780	−1.758414	0.000000
O	−0.139393	−2.870963	0.000000
O	−1.916801	−1.615098	0.000000
F	−2.411514	2.559640	0.000000
H	1.951370	−1.761070	0.000000
H	3.459303	0.227782	0.000000
H	2.475795	2.520737	0.000000
H	−0.060490	2.783010	0.000000
H	−1.497189	0.975721	0.000000

ts3

−536.6555262, No. of imaginary frequencies = 1

C	0.384238	−0.277572	−0.100308

C	−0.467640	0.748979	−0.524291
C	−1.842263	0.456677	−0.620850
C	−2.330240	−0.786297	−0.250652
C	−1.458225	−1.785939	0.237057
C	−0.099648	−1.533080	0.319560
H	−0.072945	1.698826	−0.844338
H	−2.511786	1.250164	−0.932367
H	−3.398690	−0.987359	−0.307180
H	−1.850301	−2.752102	0.547582
H	0.598618	−2.277964	0.682455
N	1.817817	−0.054149	−0.091184
O	2.551330	−0.936496	0.396527
O	2.266265	0.987504	−0.586690
F	−1.021326	2.468139	0.956752

ts4

−536.6501531, No. of imaginary frequencies = 1

C	0.138035	0.062359	−0.001845
C	0.106507	0.128199	1.393201
C	1.305717	−0.026572	2.086714
C	2.511049	−0.218262	1.395673
C	2.518966	−0.262925	−0.000155
C	1.320284	−0.119894	−0.710149
H	−0.833724	0.314073	1.890010
H	1.306702	0.041898	3.172133
H	3.442992	−0.324943	1.948441
H	3.451610	−0.407269	−0.541526
H	1.296672	−0.134029	−1.793699
N	−1.125188	0.113334	−0.745526
O	−2.157551	−0.207039	−0.152818
O	−1.078652	0.365261	−1.955535
F	−0.715700	2.381549	0.688802

mts

-536.6441744, No. of imaginary frequencies = 1

C	-0.053456	0.059916	0.047082
C	0.016768	-0.063272	1.475323
C	1.242310	-0.113306	2.128096
C	2.462067	-0.037817	1.435150
C	2.403902	0.090553	0.037361
C	1.197956	0.144082	-0.650663
H	-0.916337	-0.112921	2.027014
H	1.244207	-0.215669	3.214221
H	3.413727	-0.075927	1.960182
H	3.328880	0.150063	-0.537983
H	1.171014	0.253356	-1.729944
N	-1.108136	1.297561	-0.418127
O	-1.975225	1.660654	0.380450
O	-0.925618	1.845244	-1.508142
F	-0.971742	-0.983344	-0.564878

Fluorobenzene

-331.5012426, No. of imaginary frequencies = 0

C	0.028411	0.000000	0.016403
C	-0.004307	0.000000	1.406001
C	1.211258	0.000000	2.096955
C	2.423387	0.000000	1.399143
C	2.421645	0.000000	0.000502
C	1.215479	0.000000	-0.706730
H	-0.958516	0.000000	1.923583
H	1.207075	0.000000	3.183722
H	3.364240	0.000000	1.942345
H	3.360722	0.000000	-0.546503
H	1.186614	0.000000	-1.791891
F	-1.150133	0.000000	-0.664030

Nitrite Ion

-205.1696315, No. of imaginary frequencies = 0

N	−0.036283	0.000000	0.049685
O	0.028307	0.000000	1.312220
O	1.064527	0.000000	−0.571905

References

(S1) Clark, T.; Chandrasekhar, J.; Spitznagel, G. W.; Schleyer, P. V. R. Efficient diffuse function-augmented basis sets for anion calculations. III. The 3-21+G basis set for first-row elements, Li–F. *J. Comput. Chem.* **1983**, *4*, 294–301.

(S2) Krishnan, R.; Binkley, J. S.; Seeger, R.; Pople, J. A. Self-consistent molecular orbital methods. XX. A basis set for correlated wave functions. *J. Chem. Phys.* **1980**, *72*, 650–654.

(S3) Dunning Jr, T. H. Gaussian basis sets for use in correlated molecular calculations. I. The atoms boron through neon and hydrogen. *J. Chem. Phys.* **1989**, *90*, 1007–1023.

(S4) Kendall, R. A.; Dunning Jr, T. H.; Harrison, R. J. Electron affinities of the first-row atoms revisited. Systematic basis sets and wave functions. *J. Chem. Phys.* **1992**, *96*, 6796–6806.

(S5) Lee, C.; Yang, W.; Parr, R. G. Development of the Colle-Salvetti correlation-energy formula into a functional of the electron density. *Phys. Rev. B* **1988**, *37*, 785–789.

(S6) Becke, A. D. Density-functional thermochemistry. III. The role of exact exchange. *J. Chem. Phys.* **1993**, *98*, 5648–5652.

(S7) Zhao, Y.; Truhlar, D. G. The M06 suite of density functionals for main group thermochemistry, thermochemical kinetics, noncovalent interactions, excited states, and transition elements: two new functionals and systematic testing of four M06-class functionals and 12 other functionals. *Theor. Chem. Acc.* **2008**, *120*, 215–241.

(S8) Becke, A. D. A new mixing of Hartree–Fock and local density-functional theories. *J. Chem. Phys.* **1993**, *98*, 1372–1377.

(S9) Handy, N. C.; Cohen, A. J. Left-right correlation energy. *Mol. Phys.* **2001**, *99*, 403–412.

(S10) Hoe, W.-M.; Cohen, A. J.; Handy, N. C. Assessment of a new local exchange functional OPTX. *Chem. Phys. Lett.* **2001**, *341*, 319–328.

(S11) Perdew, J. P.; Burke, K.; Ernzerhof, M. Generalized gradient approximation made simple. *Phys. Rev. Lett.* **1996**, *77*, 3865.

(S12) Hamprecht, F. A.; Cohen, A. J.; Tozer, D. J.; Handy, N. C. Development and assessment of new exchange-correlation functionals. *J. Chem. Phys.* **1998**, *109*, 6264–6271.

(S13) Boese, A. D.; Handy, N. C. A new parametrization of exchange–correlation generalized gradient approximation functionals. *J. Chem. Phys.* **2001**, *114*, 5497–5503.

(S14) Frisch, M. J.; Trucks, G. W.; Schlegel, H. B.; Scuseria, G. E.; Robb, M. A.; Cheeseman, J. R.; Scalmani, G.; Barone, V.; Petersson, G. A.; Nakatsuji, H.; Li, X.; Caricato, M.; Marenich, A. V.; Bloino, J.; Janesko, B. G.; Gomperts, R.; Mennucci, B.; Hratchian, H. P.; Ortiz, J. V.; Izmaylov, A. F.; Sonnenberg, J. L.; Williams-Young, D.; Ding, F.; Lipparini, F.; Egidi, F.; Goings, J.; Peng, B.; Petrone, A.; Henderson, T.; Ranasinghe, D.; Zakrzewski, V. G.; Gao, J.; Rega, N.; Zheng, G.; Liang, W.; Hada, M.; Ehara, M.; Toyota, K.; Fukuda, R.; Hasegawa, J.; Ishida, M.; Nakajima, T.; Honda, Y.; Kitao, O.; Nakai, H.; Vreven, T.; Throssell, K.; Montgomery, J. A., Jr.; Peralta, J. E.; Ogliaro, F.; Bearpark, M. J.; Heyd, J. J.; Brothers, E. N.; Kudin, K. N.; Staroverov, V. N.; Keith, T. A.; Kobayashi, R.; Normand, J.; Raghavachari, K.; Rendell, A. P.; Burant, J. C.; Iyengar, S. S.; Tomasi, J.; Cossi, M.; Millam, J. M.; Klene, M.; Adamo, C.; Cammi, R.; Ochterski, J. W.; Martin, R. L.; Morokuma, K.; Farkas, O.; Foresman, J. B.; Fox, D. J. Gaussian~16 Revision C.01. 2016; Gaussian Inc. Wallingford CT.

(S15) Riplinger, C.; Neese, F. An efficient and near linear scaling pair natural orbital based local coupled cluster method. *J. Chem. Phys.* **2013**, *138*, 034106.

(S16) Riplinger, C.; Sandhoefer, B.; Hansen, A.; Neese, F. Natural triple excitations in local coupled cluster calculations with pair natural orbitals. *J. Chem. Phys.* **2013**, *139*, 134101.

(S17) Neese, F. The ORCA program system. *Wiley Interdiscip. Rev. Comput. Mol. Sci.* **2012**, *2*, 73–78.

(S18) Okoshi, M.; Atsumi, T.; Nakai, H. Revisiting the extrapolation of correlation energies to complete basis set limit. *J. Comput. Chem.* **2015**, *36*, 1075–1082.

(S19) Sun, L.; Hase, W. L. *Reviews in Computational Chemistry, Vol. 19*; John Wiley & Sons, Ltd, 2003; Chapter 3, pp 79–146.

(S20) Lourderaj, U.; Sun, R.; Kohale, S. C.; Barnes, G. L.; de Jong, W. A.; Windus, T. L.; Hase, W. L. The VENUS/NWChem software package. Tight coupling between chemical dynamics simulations and electronic structure theory. *Comput. Phys. Commun.* **2014**, *185*, 1074–1080.

(S21) Valiev, M.; Bylaska, E. J.; Govind, N.; Kowalski, K.; Straatsma, T. P.; Van Dam, H. J.; Wang, D.; Nieplocha, J.; Apra, E.; Windus, T. L., et al. NWChem: A comprehensive and scalable open-source solution for large scale molecular simulations. *Comput. Phys. Commun.* **2010**, *181*, 1477–1489.

(S22) Giroldo, T.; Xavier, L. A.; Riveros, J. M. An unusually fast nucleophilic aromatic displacement reaction: The gas-phase reaction of fluoride ions with nitrobenzene. *Angew. Chem. Int. Ed.* **2004**, *43*, 3588–3590.

(S23) Hare, S. R.; Bratholm, L. A.; Glowacki, D. R.; Carpenter, B. K. Low dimensional representations along intrinsic reaction coordinates and molecular dynamics trajectories using interatomic distance matrices. *Chem. Sci.* **2019**, *10*, 9954–9968.

(S24) Tsutsumi, T.; Ono, Y.; Arai, Z.; Taketsugu, T. Visualization of the Dynamics Effect: Projection of on-the-Fly Trajectories to the Subspace Spanned by the Static Reaction Path Network. *J. Chem. Theory Comput.* **2020**, *16*, 4029–4037.